Nonlinear Dyn (2012) 67:2899–2908
DOI 10.1007/s11071-011-0197-x

ORIGINAL PAPER

Effect of high-frequency stimulation on nerve pulse propagation in the FitzHugh–Nagumo model

Irmantas Ratas · Kestutis Pyragas

Received: 16 May 2011 / Accepted: 8 August 2011 / Published online: 11 September 2011

Abstract We consider the FitzHugh–Nagumo model axon under action of a homogeneous high-frequency stimulation (HFS) current. Using a multiple scale method and a geometrical singular perturbation theory, we derive analytically the main characteristics of the traveling pulse. We show that the effect of HFS on the axon is determined by a parameter proportional to the ratio of the amplitude to the frequency of the stimulation current. When this parameter is increased, the pulse slows down and shrinks. At some threshold value, the pulse stops and its width becomes zero. The HFS prevents the pulse propagation when the parameter exceeds the threshold value. The analytical results are confirmed by numerical experiments performed with the original system of partial differential equations.

Keywords High-frequency stimulation · FitzHugh–Nagumo model · Traveling pulse · Multiple scale method · Singular perturbation theory

1 Introduction

Although applied electrical stimulation was used to characterize neural activity for over 200 years, only in recent decades it has been moved beyond the realm of inquisitive exploration into clinical application. Undesirable hyper-activity of neurons characterizes many diseases and may cause pathological motor or sensory effects. Blocking these action potentials could help alleviate pain or stop muscle spasms [1, 2]. High-frequency alternating currents (HFAC) applied directly to the nerve, has been experimentally shown to produce a reversible conduction block [3–8]. Some theoretical understanding of this phenomenon has been achieved by numerical simulations of the Hodgkin–Huxley type axon models with a locally applied HFAC [7–10].

High-frequency electrical stimulation has been also applied clinically via deep brain stimulation (DBS) electrodes implanted in specific brain regions to treat movement disorders such as Parkinson's disease and dystonia [11–14]. In addition, DBS therapies have been explored for other neurological disorders including depression and epilepsy [15, 16]. Despite a long and successful history of using DBS therapy, its mechanism of action is still unclear [17, 18]. Some experiments in animals show that high-frequency DBS can block axonal conduction [19, 20] and this might explain the mechanism of its therapeutic action. The size of electrodes used clinically for DBS are large macroelectrodes, several orders of magnitude larger than single neuron cells [21]. Therefore, the models of locally applied HFAC [7–10] are not appropriate for this situation. More suitable description of action of DBS electrode may be based on a hypothesis that the DBS elec-

I. Ratas (✉) · K. Pyragas
Center for Physical Sciences and Technology,
Semiconductor Physics Institute, 01108 Vilnius, Lithuania
e-mail: irmantas.ff.vu@gmail.com

trode provides a homogeneous high-frequency stimulation along the whole axon. Investigation of such models is essential for better understanding the ability of axons to propagate pulses under action of DBS.

In this paper, we analyze the effect of a homogeneous HFS on pulse propagation in a single axon. We consider an axon model described by the FitzHugh–Nagumo (FN) equations [22, 23] and show that for sufficiently large amplitudes of HFS the pulses cannot propagate in the axon. Seeking analytical results we first apply a multiple-scale method [24] and separate the neuron dynamics into slow and fast components. As a result, we derive averaged equations for the slow component that do not contain a high-frequency term. Then we analyze the traveling waves in the averaged system via a singular perturbation theory [25, 26]. Such an approach allows us to obtain the dependence of the parameters of the traveling pulse on the amplitude of HFS current in an analytical form and derive an analytical formula for the threshold of conduction block.

The rest of the paper is organized as follows. In Sect. 2, we formulate the problem and reduce the FN model under HFS to averaged equations. Section 3 is devoted to analytical and numerical analysis of traveling pulse solutions of the averaged system. In Sect. 4, we justify the results of traveling pulse solutions by numerical experiments performed with the original FN model and averaged equations. The paper is finished with the conclusions presented in Sect. 5.

2 Model equations and averaged system

Let us consider the FitzHugh–Nagumo model neuron [22, 23] in the presence of homogeneously applied HFS current:

$$\frac{\partial v}{\partial t} = v - \frac{v^3}{3} - w + D\frac{\partial^2 v}{\partial x^2} + a\cos(\omega t), \tag{1a}$$

$$\frac{\partial w}{\partial t} = \varepsilon(v + \beta - \gamma w). \tag{1b}$$

Here, (1a) describes the dynamics of the membrane potential v, where D is the diffusion coefficient and parameters a and ω define respectively the amplitude and frequency of HFS induced by DBS electrode. Equation (1b) defines the dynamics of the slow recovery variable w with a positive rate parameter $\varepsilon \ll 1$. The parameters β and γ are chosen such that without of HFS ($a = 0$) the neuron is in an excitable regime. In numerical simulations presented below, we fix $\beta = 0.7$ and $\gamma = 0.8$. The diffusion coefficient D can be eliminated by rescaling the space variable x, and thus in the following we take $D = 1$ without loss of generality.

If the period $T = 2\pi/\omega$ of HFS is much less than all characteristic times of the FN neuron, then the system (1) can be solved by a multiple-scale method [24], or more precisely, by a two-scale expansion. According to this method, an approximate solution of the system (1) can be represented as a sum of slow and fast components (see the Appendix for details):

$$v(t) \approx \bar{v}(t) + A\sin(\omega t), \tag{2a}$$

$$w(t) \approx \bar{w}(t), \tag{2b}$$

where the slow variables are marked by bars and

$$A = \frac{a}{\omega}. \tag{3}$$

is the main parameter defining an action of the HFS. In the following, we refer to this parameter as the stimulation parameter. This parameter is proportional to the ratio of the amplitude a to the frequency ω of HFS. From (2), we see that the fast high-frequency component $A\sin(\omega t)$ is added only to the membrane potential and the recovery variable contains only the slow component. The slow variables $\bar{v}(t)$ and $\bar{w}(t)$ describe the dynamics of the system averaged over the period of stimulation and satisfy the equations:

$$\frac{\partial \bar{v}}{\partial t} = \bar{v}\left(1 - \frac{A^2}{2}\right) - \frac{\bar{v}^3}{3} - \bar{w} + \frac{\partial^2 \bar{v}}{\partial x^2}, \tag{4a}$$

$$\frac{\partial \bar{w}}{\partial t} = \varepsilon(\bar{v} + \beta - \gamma\bar{w}). \tag{4b}$$

Formally, these equations are similar to the original system (1) (for $a = 0$ they are identical), but the HFS term $a\cos(\omega t)$ is eliminated in (4). The dependence of the averaged system (4) on the HFS appears through the modification of the coefficient at the variable $\bar{v}$ in the r.h.s. of (4a). As a result, the nullcline of this equation becomes dependent on the stimulation parameter A. The nullclines for different values of A are shown in Fig. 1, while the inset of this figure shows the dependence of the excitability parameter Δ on A. The definition of the excitability parameter Δ is evident from Fig. 1. We see that the increase of the stimulation parameter A reduces the excitability of the neuron, since for sufficiently large A the parameter Δ increases drastically with the increase of A. Thus, we

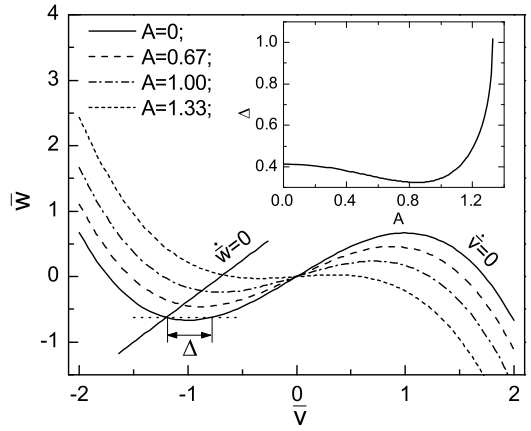

Fig. 1 The nulclines [$\dot{\bar{w}} = 0$: $\bar{w} = (\bar{v} + \beta)/\gamma$ and $\dot{\bar{v}} = 0$: $\bar{w} = \bar{v}(1 - A^2/2) - \bar{v}^3/3$] of the averaged system (4) for different values of the stimulation parameter A. The *inset* shows the dependence of the excitability parameter Δ on A

can expect the large stimulation intensities to block the propagation of pulses. In the next section, we derive the precise criterion for such a conduction block phenomenon.

3 Traveling pulse solutions of the averaged system

To study traveling waves, we first place the system of equations (4) in a traveling coordinate frame of reference. We define the traveling wave coordinate $\xi = x - ct$, where $c > 0$ is the wave speed, yet to be determined. Then the partial differential equations (4) for the stationary traveling waves become the ordinary differential equations:

$$\bar{v}_\xi = \bar{u}, \tag{5a}$$

$$\bar{u}_\xi = -\bar{v}\left(1 - \frac{A^2}{2}\right) + \frac{\bar{v}^3}{3} + \bar{w} - c\bar{u}, \tag{5b}$$

$$\bar{w}_\xi = -\frac{\varepsilon}{c}(\bar{v} + \beta - \gamma\bar{w}). \tag{5c}$$

Here, the subscript ξ denotes the derivative with respect to the traveling wave coordinate ξ and an auxiliary variable $\bar{u} \equiv \bar{v}_\xi$ is introduced to write the system as first order differential equations. This system has the only fixed point $(\bar{v}_0, \bar{u}_0, \bar{w}_0)$ with the coordinates $\bar{u}_0 = 0$, $\bar{w}_0 = (\bar{v}_0 + \beta)/\gamma$ and $\bar{v}_0$ being the resting potential of the neuron that satisfies the real value solution of the cubic equation

$$\frac{\bar{v}_0^3}{3} - \bar{v}_0\left(1 - \frac{1}{\gamma} - \frac{A^2}{2}\right) + \frac{\beta}{\gamma} = 0. \tag{6}$$

The traveling pulse solutions are defined by homoclinic orbits of system (5). Such orbits begin and end at the fixed point of the system. For further analysis, it is convenient to shift the origin of the coordinate system of equations (5) to the fixed point. Then the equations for the deviations from the fixed point $(\delta v, \delta u, \delta w) = (\bar{v} - v_0, \bar{u} - u_0, \bar{w} - w_0)$ read:

$$\delta v_\xi = \delta u, \tag{7a}$$

$$\delta u_\xi = (A^2/2 - 1 + \bar{v}_0^2)\delta v + \bar{v}_0\delta v^2 + \delta v^3/3 + \delta w - c\delta u, \tag{7b}$$

$$\delta w_\xi = -(\delta v - \gamma\delta w)\varepsilon/c. \tag{7c}$$

3.1 Traveling pulses in a singular limit $\varepsilon \to 0$

To find approximate analytical expressions for the traveling pulse, one can use perturbation methods exploiting the different time scales of the system. In the limit of small parameter $\varepsilon \to 0$, the traveling pulse can be constructed with the help of the geometrical singular perturbation theory [25, 26]. The phase space sketch of homoclinic orbits for system (7) in the singular limit $\varepsilon = 0$ is presented in Fig. 2(a). There are two homoclinic orbits marked by letters U and S. The first orbit lies completely in the plane $\delta w = 0$ and describes a pulse with the zero velocity, which is unstable [27], and hence is not interesting from a physical point of view. The second orbit marked by letter S represents a traveling pulse, which is of interest for further analysis, since it is stable [28]. In Fig. 2(b), a voltage pulse sketch of this orbit is shown in the traveling coordinate frame for small $\varepsilon > 0$. Going backward in ξ or forward in time this pulse consists of four segments [25, 26]: (i) The leading edge that corresponds to a fast dynamics in the plane $\delta w = 0$ of the phase space of system (7) [cf. Fig. 2(a)]; (ii) A slow relaxation from $\delta w = 0$ to a new value $\delta w = \delta\tilde{w} = \text{const.}$ at the conditions $\delta u = 0$ and $\delta u_\xi = 0$; (iii) The trailing edge that corresponds to a fast dynamics in the plane $\delta w = \delta\tilde{w}$; (iv) The slow relaxation from $\delta w = \delta\tilde{w}$ back to zero at the conditions $\delta u = 0$ and $\delta u_\xi = 0$. Below we describe the governing equations for each segment of the homoclinic trajectory in more details, and derive the main parameters of the traveling pulse.

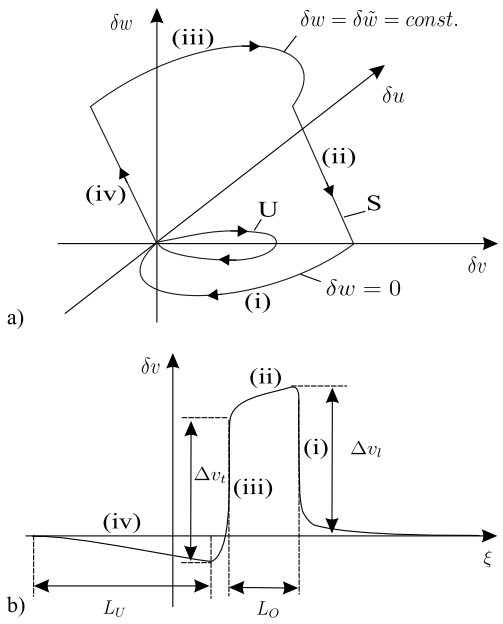

Fig. 2 (**a**) Phase space sketch of stable (S) and unstable (U) homoclinic trajectories of system (7) in a singular perturbation limit $\varepsilon = 0$. (**b**) Voltage pulse of the stable (S) homoclinic orbit vs. traveling wave coordinate ξ for small $\varepsilon > 0$. Δv_l and Δv_s denote the heights of the leading and trailing edges while L_O and L_U mark respectively the lengths of pulse segments corresponding to the overshoot and undershoot

(i) *The leading edge.* This segment of the homoclinic trajectory lies in the plane $\delta w = 0$ and the dynamics of fast variables δv and δu is governed by (7a) and (7b) that can be presented in the form

$$\delta v_\xi = \delta u, \tag{8a}$$

$$\delta u_\xi = \delta v(\delta v - \delta v_1)(\delta v - \delta v_2)/3 - c\delta u \tag{8b}$$

with

$$\delta v_{1,2} = \left[-3\bar{v}_0 \pm \left(12 - 6A^2 - 3\bar{v}_0^2\right)^{1/2}\right]/2. \tag{9}$$

The leading edge is defined by heteroclinic trajectory of the system (8), which connects its fix points $(0, 0)$ and $(\delta v_1, 0)$ in the phase plane $(\delta v, \delta u)$. Such a trajectory exists when the speed c satisfies (cf., for example, Ref. [29], p. 273):

$$c = \sqrt{1/6}(\delta v_1 - 2\delta v_2). \tag{10}$$

Although here we have determined the speed of the leading edge, (10) defines the speed of the whole pulse, since the speed of all segments of the traveling pulse must be the same. The dependence of the

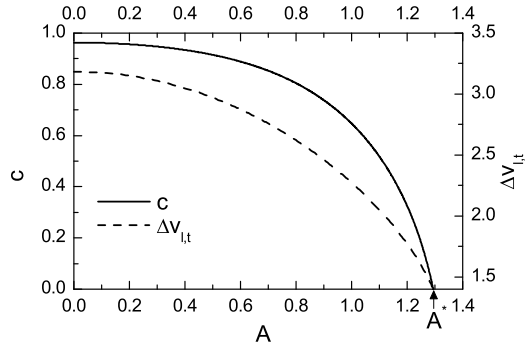

Fig. 3 Pulse speed c and heights of leading Δv_l and trailing Δv_t edges ($\Delta v_l = \Delta v_t$) as functions of the stimulation parameter A

speed c on the stimulation parameter A can be defined analytically in a parametric form. For this purpose, we choose the resting potential $\bar{v}_0$ as an independent, variable parameter. Then the dependence of A on $\bar{v}_0$ can be obtained from (6)

$$A(\bar{v}_0) = \left[2\left(1 - 1/\gamma - \bar{v}_0^2/3 - \beta/\gamma\,\bar{v}_0\right)\right]^{1/2}. \tag{11}$$

The speed c in (10) is expressed through variables δv_1 and δv_2 whose dependence on the parameter $\bar{v}_0$ is determined by (9). Thus, the parametric dependence of the speed on the stimulation parameter $[c = c(\bar{v}_0), A = A(\bar{v}_0)]$ is defined by (9)–(11). This dependence is depicted in Fig. 3. We see that the speed of traveling pulse decreases with the increase of stimulation intensity and turns to zero at a critical value $A = A^*$ defined by

$$A^* = \sqrt{2(1 - \beta^2/3)}. \tag{12}$$

The zero speed is attained at the resting potential $\bar{v}_0 = -\beta$. Equation (12) defines a threshold stimulation intensity for existence of traveling pulse. For $A > A^*$, the traveling pulse solution does not exist, and thus the pulses cannot propagate in the axon if the amplitude a of HFS exceeds the critical value $a^* = \omega A^*$, which is proportional to the frequency of HFS.

The hight Δv_l of the leading edge [cf. Fig. 2(b)] is defined as $\Delta v_l = \delta v_1$. Its parametrical dependence on the stimulation parameter A is determined by equations (9) and (11) and is shown in Fig. 3. The hight Δv_l decreases with the increase of the stimulation parameter A, however, unlike the velocity it does not vanish when the stimulation parameter reaches the critical value A^*.

(ii) *Slow relaxation from* $\delta w = 0$ *to* $\delta w = \delta\tilde{w}$. Here, one can neglect the variation of the fast variables in system (7), taking $\delta v_\xi = 0$ and $\delta u_\xi = 0$. It follows that $\delta u = 0$ and δw is related with δv by

$$\delta w = F(\delta v) \equiv -\delta v(\delta v - \delta v_1)(\delta v - \delta v_2)/3. \tag{13}$$

The dynamics of the slow variable δw is determined by (7c) with the initial condition $\delta w = 0$ and relationship between the variables δw and δv defined by (13). We are interesting in the length L_O of this segment (pulse overshoot) [cf. Fig. 2(b)], which can be defined as

$$L_O = \frac{c}{\varepsilon}\int_{\delta\tilde{w}}^{0} \frac{d\delta w}{\gamma\delta w - \delta v}. \tag{14}$$

Note that the value $\delta\tilde{w}$ is jet unknown; it will be determined in the next segment of the homoclinic trajectory.

(iii) *The trailing edge.* This segment of trajectory lies in the plane $\delta w = \delta\tilde{w}$. Here, the dynamics of fast variables δv and δu is governed by (7a) and (7b) that can be presented in the form

$$\delta v_\xi = \delta u, \tag{15a}$$

$$\delta u_\xi = \Phi(\delta v, \delta\tilde{w}) - c\delta u, \tag{15b}$$

where

$$\Phi(\delta v, \delta\tilde{w}) = \delta v(\delta v - \delta v_1)(\delta v - \delta v_2)/3 + \delta\tilde{w} \tag{16}$$

is a third order polynomial with respect to the variable δv. Denote the roots of this polynomial as $\delta\tilde{v}_1 < \delta\tilde{v}_2 < \delta\tilde{v}_3$ and rewrite (16) in the form:

$$\Phi(\delta v, \delta\tilde{w}) = (\delta v - \delta\tilde{v}_1)(\delta v - \delta\tilde{v}_2)(\delta v - \delta\tilde{v}_3)/3. \tag{17}$$

The trailing edge is defined by heteroclinic trajectory of the system (15), which connects its fix points $(\delta\tilde{v}_3, 0)$ and $(\delta\tilde{v}_1, 0)$ in the phase plane $(\delta v, \delta u)$. Such a trajectory exists when the speed c [which must coincide with the speed of the leading edge defined by (10)] satisfies

$$c = \sqrt{1/6}(2\delta\tilde{v}_2 - \delta\tilde{v}_3 - \delta\tilde{v}_1). \tag{18}$$

Comparing (17) with (16) and (18) with (10), we obtain the relationship between the coordinates of fixed points of systems (15) and (8)

$$\delta\tilde{v}_1 = (2\delta v_2 - \delta v_1)/3, \tag{19a}$$

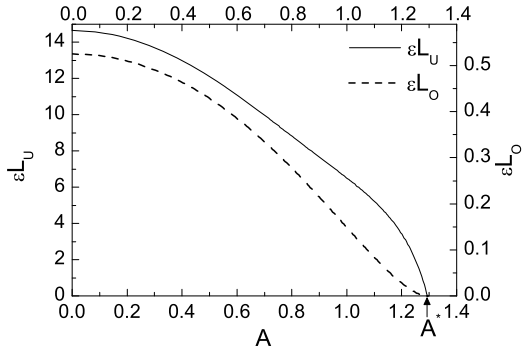

Fig. 4 The lengths of pulse overshoot (L_O) and undershoot (L_U) multiplied by parameter ε vs. the stimulation parameter A

$$\delta\tilde{v}_2 = (2\delta v_1 - \delta v_2)/3, \tag{19b}$$

$$\delta\tilde{v}_3 = 2(\delta v_1 + \delta v_2)/3 \tag{19c}$$

and define the value of unknown parameter $\delta\tilde{w}$ introduced previously:

$$\delta\tilde{w} = -\delta\tilde{v}_1\delta\tilde{v}_2\delta\tilde{v}_3/3. \tag{20}$$

The hight Δv_l of the trailing edge [cf. Fig. 2(b)] is defined as $\Delta v_t = \delta\tilde{v}_3 - \delta\tilde{v}_1$. From (19a) and (19c), it is easy to see that it coincides with the hight of the leading edge, $\Delta v_t = \delta v_1 = \Delta v_l$.

Taking into account the above results, (14) defining the length of the pulse overshoot can be rewritten in a form convenient for numerical estimation,

$$L_O = \frac{c}{\varepsilon}\int_{\delta\tilde{v}_3}^{\delta v_1} \frac{F'(\delta v)\,d\delta v}{\gamma F(\delta v) - \delta v}, \tag{21}$$

where $F'(\delta v)$ is the derivative of function $F(\delta v)$. Here, we have replaced the integration variable δw by δv taking into account the relationship (13).

(iv) *Slow relaxation from* $\delta w = \delta\tilde{w}$ *back to* $\delta w = 0$. Here as well as in the segment (ii), the variation of fast variables is neglected and dynamics of the slow variable δw is determined by (7c) with the initial condition $\delta w = \delta\tilde{w}$. Taking into account the relationship (13) between the variables δw and δv the length L_U of this segment (pulse undershoot) [cf. Fig. 2(b)] is defined by integral:

$$L_U = \frac{c}{\varepsilon}\int_{0}^{\delta\tilde{v}_1} \frac{F'(\delta v)\,d\delta v}{\gamma F(\delta v) - \delta v}. \tag{22}$$

The lengths L_O and L_U are shown in Fig. 4 as functions of the stimulation parameter A. Both lengths

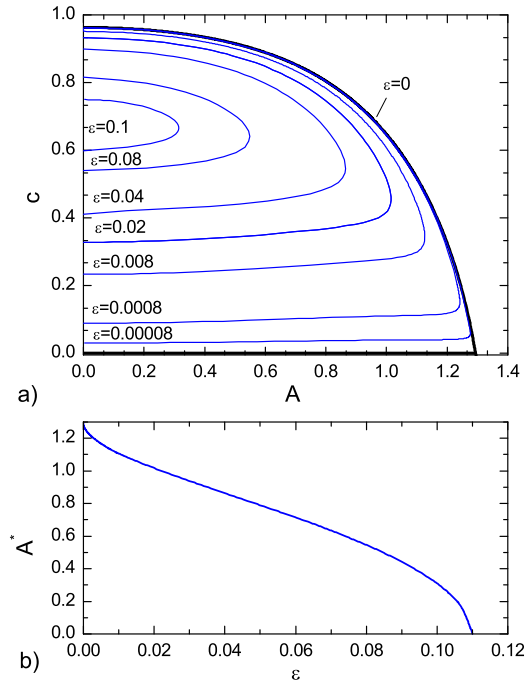

Fig. 5 (**a**) The speed c of traveling pulses as a function of the stimulation parameter A for different values of ε. The *bold curves* show the speed dependence analytically determined in the singular perturbation limit $\varepsilon = 0$. (**b**) The threshold A^* of the stimulation parameter vs. ε

decrease with the increase of A and vanish when the stimulation parameter reaches the threshold value A^*. Thus, the mechanism of HFS responsible for the suppression of pulse propagation consists in pulse narrowing. With the increase of HFS intensity, the pulse shrinks and its width becomes zero when $A = A^*$.

3.2 Traveling pulses for finite $\varepsilon > 0$

The singular perturbation theory has allowed us to determine analytically many important characteristics of the traveling pulse, including the threshold value A^* of the stimulation parameter for the existence of traveling pulse solution. In fact, the threshold A^* depends on the parameter ε. For finite $\varepsilon > 0$, the analytical approach fails and the homoclinic trajectories of system (7) can be determined only numerically. In Fig. 5, we show the results of such an analysis. The dependence of the pulse speed on the stimulation parameter A for different values of ε is presented in Fig. 5(a). For $\varepsilon \geq 0.008$, these curves have been constructed with the help of the MatCont package [30] and for smaller $\varepsilon \leq 0.0008$, the shooting method [31] has been used. Each curve consists of two branches. The upper branch represents the speed of the stable pulse [27], while the lower branch corresponds to the unstable pulse [28]. The point where the two branches coincide defines the threshold parameter A^*. At this point, the homoclinic trajectories corresponding to the fast (stable) and slow (unstable) pulses collide and disappear, such that for $A > A^*$ the traveling pulse solutions do not exist. Note that the curves in Fig. 5(a) approach asymptotically the singular perturbation solution (bold curve) when $\varepsilon \to 0$. This justifies the analytical results obtained in the previous section.

The dependence of the threshold A^* of the stimulation parameter on ε is shown in Fig. 5(b). Larger values of the parameter ε require less stimulation intensity A^* to suppress the pulse. This is because the pulse length of the free ($A = 0$) system depends on the parameter ε. The increase of the parameter ε has the same effect as the increase of the stimulation intensity A; they both narrow the pulse [cf. (21) and (22)]. Therefore, for larger ε, less HFS intensity is needed to zero the pulse length and suppress its propagation.

4 Numerical experiments

To justify the results of stationary traveling pulse solutions obtained in the previous section, here we perform numerical experiments with the original system (1) of partial differential equations (PDE) as well as with the averaged PDEs (4). First, we verify the validity of the averaged equations. In Fig. 6, we show the dynamics of the neuron potential in the middle of the sample at different values of the stimulation parameter A. The thin (blue) curves represent the solutions of the original system (1) while the bold (red) curves show the solutions of the averaged equations (4). We see that these solutions are in good agreement. The PDEs have been solved with the periodic boundary conditions taking the length of the sample equal to $L = 400$. The initial conditions are chosen in such a way, that for a given stimulation intensity A, they coincide with the stable pulse profile. As predicted by singular perturbation theory and numerical analysis of stationary pulses for finite ε, the increase of the stimulation intensity leads to the decrease of both the pulse velocity and the pulse length [cf. Figs. 6(a)–(c)]. The propagating pulse disappears for $A > A^* \approx 1.13$ and only small amplitude subthreshold high-frequency oscillations remain [cf. Fig. 6(d)].

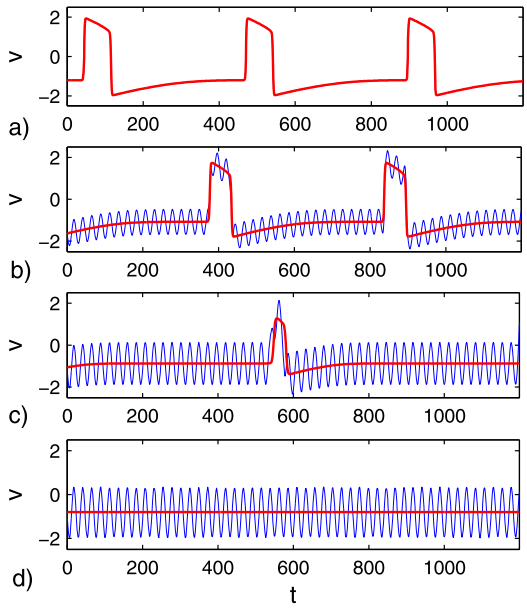

Fig. 6 The dynamics of the neuron potential at the middle of the sample for fixed $\varepsilon = 0.008$ and $\omega = 50$, and different values of the HFS amplitudes: (**a**) $a = 0$ ($A = 0$); (**b**) $a = 30$ ($A = 0.6$); (**c**) $a = 50$ ($A = 1$); (**d**) $a = 56.5$ ($A = 1.13$). The *thin* (*blue*) *curves* show the solutions of the original system (1) and the *bold* (*red*) *curves* represent the solutions of the averaged system (4)

In Fig. 7, we demonstrate the space-time evolution of the averaged system (4) under initial excitation of the middle of the neuron. The excitation is performed with a DC current $I = 2$ applied to the small space interval $\Delta x = 4$ in the center of the sample for the initial time interval $\Delta t = 1$; then the DC current is off. In the absence of HFS, the DC stimulus initiates two pulses traveling in opposite directions [cf. Fig. 7(a)]. An influence of HFS to the pulse propagation is demonstrated in Figs. 7(b)–(d). When the HFS intensity is increased, the propagating pulses shrink and slow down. The pulses die out when the stimulation parameter exceeds the threshold value $A^* \approx 1.13$ [cf. Fig. 7(d)]. Again, this confirms the main conclusions of the previous section.

5 Conclusions

We have analyzed the effect of a homogeneous high-frequency stimulation on a nerve pulse propagation in the framework of a simple FitzHugh–Nagumo model axon. Exploiting the multiple-scale method and geometrical singular perturbation theory, we managed to derive the main characteristics of the traveling pulse

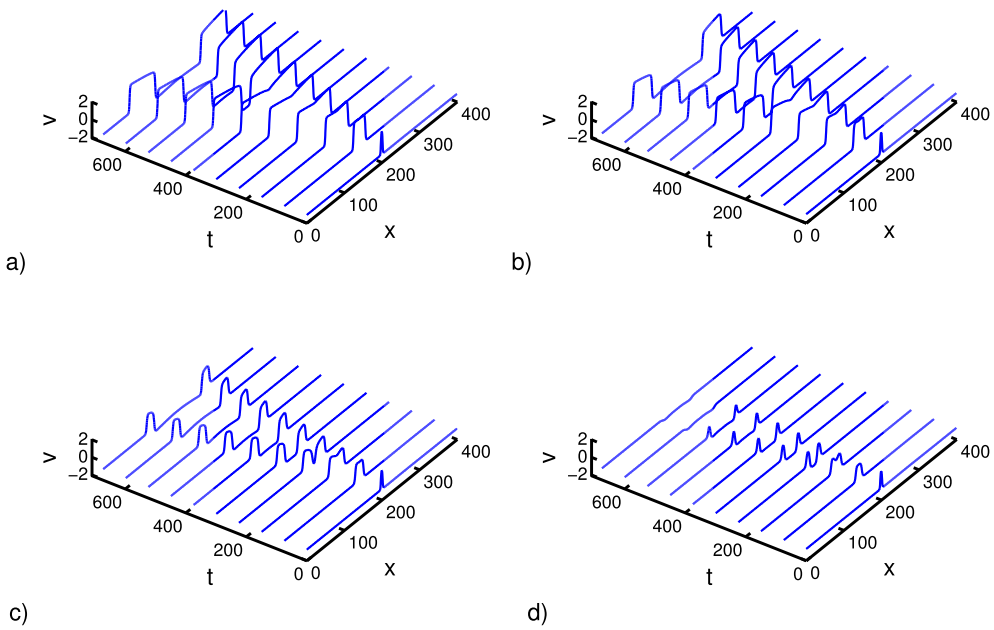

Fig. 7 Space-time evolution of the averaged system (4) under initial excitation of the center of the neuron with the DC current $I = 2$ applied for a short time interval $\Delta t = 1$. The parameter ε is the same as in Fig. 6 and the HFS amplitudes are: (**a**) $A = 0$; (**b**) $A = 0.6$; (**c**) $A = 1.0$; (**d**) $A = 1.13$

under action of high-frequency stimulation in an analytical form. We have shown that the axon dynamics can be presented as a sum of slow and fast components and for the slow component derived a system of averaged equations. In this approximation, the effect of high-frequency stimulation on the axon is determined by the parameter equal to the ratio of the amplitude to the frequency of the stimulation current.

A homogeneous high-frequency stimulation is an efficient tool to control the width and velocity of the traveling pulse. With the increase of the stimulation amplitude, the pulse shrinks and slows down. Our analytical approach has allowed us to understand the mechanism of conduction block. When the stimulation amplitude riches the threshold value, the pulse stops and disappears through a zero width. The further increase of the stimulation amplitude prevents the pulse to propagate through the axon. An obtained analytical expression for the threshold of conduction bock shows that the threshold amplitude preventing the pulse propagation increases linearly with the frequency of stimulation current. This is in agreement with numerical simulations of conduction block effects in more complex and more realistic axon models considered in [8, 10]. Our analytical results are also confirmed by numerical experiments performed with the original system of partial differential equations describing the FitzHugh–Nagumo axon under HFS.

The obtained results are relevant to the DBS research, since they demonstrate an influence of a homogeneous HFS on nerve pulse propagation in an axon. Our analysis suggests that axons located in the vicinity of DBS electrode experience drastic changes; the pulses propagating through these axons may be narrowed and their speed may be reduced. For sufficiently large stimulation intensity, the axons can be blocked. These changes in axonal conductivity may be responsible for the therapeutic effect of high-frequency DBS.

Acknowledgements This work was supported by the Global grant No. VP1-3.1-ŠMM-07-K-01-025.

Appendix: Derivation of averaged equations for HF stimulated FitzHugh–Nagumo model

In the presence of HFS, (1) can be solved approximately by a multiple-scale method [24], or more precisely, by a two-scale expansion. We assume the frequency ω of the HFS to be a large parameter. In other words, the time ω^{-1} is much less than all characteristic time-scales of the system. Since the HFS is nonresonant, it provides an appreciable effect on the system dynamics only for sufficiently large amplitude a. In the following, we suppose that a is proportional to the frequency ω, $a = A\omega$, where the parameter A is independent of ω. We introduce a fast time $\tau = \omega t$ (the time t is respectively called a slow time) and expand the solution of the system (1) in powers of small parameter ω^{-1}:

$$v(t) = v_0(t,\tau) + \omega^{-1} v_1(t,\tau) + \cdots, \tag{23a}$$

$$w(t) = w_0(t,\tau) + \omega^{-1} w_1(t,\tau) + \cdots. \tag{23b}$$

We suppose that the functions $v_0(t,\tau)$, $v_1(t,\tau)$, $w_0(t,\tau)$ and $w_1(t,\tau)$ are 2π periodic in τ. This means that the solution is periodic on the fast time scale with the period equal to the period of HFS. We treat t and τ as if they where independent variables and obtain

$$\frac{\partial v}{\partial t} = \omega \frac{\partial v_0}{\partial \tau} + \frac{\partial v_0}{\partial t} + \frac{\partial v_1}{\partial \tau} + \cdots, \tag{24a}$$

$$\frac{\partial w}{\partial t} = \omega \frac{\partial w_0}{\partial \tau} + \frac{\partial w_0}{\partial t} + \frac{\partial w_1}{\partial \tau} + \cdots. \tag{24b}$$

Substituting (23) and (24) into (1) and equating terms proportional to ω^1, we obtain

$$\frac{\partial v_0}{\partial \tau} = A\sin(\tau), \tag{25a}$$

$$\frac{\partial w_0}{\partial \tau} = 0. \tag{25b}$$

Similarly, for terms proportional to ω^0, we get

$$\frac{\partial v_0}{\partial t} + \frac{\partial v_1}{\partial \tau} = v_0 - \frac{v_0^3}{3} - w_0 + \frac{\partial^2 v_0}{\partial x^2}, \tag{26a}$$

$$\frac{\partial w_0}{\partial t} + \frac{\partial w_1}{\partial \tau} = \varepsilon(v_0 + \beta - \gamma w_0). \tag{26b}$$

As pointed out in Sect. 2, we assume $D = 1$ without loss of generality. The solution of (25) is

$$v_0(t,\tau) = \bar{v}(t) + A\cos(\tau), \tag{27a}$$

$$w_0(t,\tau) = \bar{w}(t), \tag{27b}$$

where $\bar{v}(t)$ and $\bar{w}(t)$ are jet unknown functions of the slow time t. The equations for these functions are ob-

tained by substituting (27) into (26)

$$\frac{\partial \bar{v}}{\partial t} + \frac{\partial v_1}{\partial \tau} = \bar{v} + A\cos(\tau) - \frac{(\bar{v} + A\cos(\tau))^3}{3} - \bar{w} + \frac{\partial^2 \bar{v}}{\partial x^2}, \tag{28a}$$

$$\frac{\partial \bar{w}}{\partial t} + \frac{\partial w_1}{\partial \tau} = \varepsilon(\bar{v} + A\cos(\tau) + \beta - \gamma \bar{w}). \tag{28b}$$

and averaging these equations over the period 2π of the fast time τ:

$$\frac{\partial \bar{v}}{\partial t} = \bar{v}\left(1 - \frac{A^2}{2}\right) - \frac{\bar{v}^3}{3} + \frac{\partial^2 \bar{v}}{\partial x^2}, \tag{29a}$$

$$\frac{\partial \bar{w}}{\partial t} = \varepsilon(\bar{v} + \beta - \gamma \bar{w}). \tag{29b}$$

Finally, an approximate solution of (1) is

$$v(t) \approx \bar{v}(t) + A\sin(\omega t), \tag{30a}$$

$$w(t) \approx \bar{w}(t), \tag{30b}$$

where $A = a/\omega$ and the functions $\bar{v}(t)$ and $\bar{w}(t)$ satisfy the averaged equations (29). Note that the effect of HFS on the averaged neuron dynamics is completely determined by the parameter A, which is proportional to the ratio of the amplitude a to the frequency ω of stimulation current.

References

1. Long, D.M.: Electrical stimulation for the control of pain. Arch. Surg. **112**, 884–888 (1977)
2. Nashold, B.S., Goldner, J.L., Mullen, J.B., Bright, D.S.: Long-term pain control by direct peripheral-nerve stimulation. J. Bone Jt. Surg., Am. Vol. **64**, 1–10 (1982)
3. Woo, M.Y., Campbell, B.: Asynchronous firing and block of peripheral nerve conduction by 20 kc alternating current. Bull. Los Angel. Neurol. Soc. **29**, 87–94 (1964)
4. Bowman, B.R., McNeal, D.R.: Response of single alpha motoneurons to high-frequency pulse trains. Firing behavior and conduction block phenomenon. Appl. Neurophysiol. **49**, 121–138 (1986)
5. Kilgore, K., Bhadra, N.: Nerve conduction block utilizing high-frequency alternating current. Med. Biol. Eng. Comput. **42**, 394–406 (2004)
6. Bhadra, N., Kilgore, K.L.: High-frequency electrical conduction block of mammalian peripheral motor nerve. Muscle Nerve **32**, 782–790 (2005)
7. Williamson, R.P., Andrews, B.J.: Localized electrical nerve blocking. IEEE Trans. Biomed. Eng. **52**, 362–370 (2005)
8. Kilgore, K.L., Bhadra, N.: High frequency mammalian nerve conduction block: simulations and experiments. In: Conf. Proc. IEEE Eng. Med. Biol. Soc., New York City, USA, vol. 1, pp. 4971–4974 (2006)
9. Rattay, F.: Electrical Nerve Stimulation; Theory, Experiments and Applications. Springer, Wien, New York (1990)
10. Tai, C., de Groat, W.C., Roppolo, J.R.: Simulation of nerve block by high-frequency sinusoidal electrical current based on the Hodgkin–Huxley model. IEEE Trans. Neural Syst. Rehabil. Eng. **13**, 415–422 (2005)
11. Benabid, A.L., Pollak, P., Gervason, C., Hoffmann, D., Gao, D.M., Hommel, M., Perret, J.E., de Rougemont, J.: Long-term suppression of tremor by chronic stimulation of the ventral intermediate thalamic nucleus. Lancet **337**, 403–406 (1991)
12. Benabid, A.L., Benazzouz, A., Hoffmann, D., Limousin, P., Krack, P., Pollak, P.: Long-term electrical inhibition of deep brain targets in movement disorders. Mov. Disord., **13**, 119–125 (1998)
13. Yianni, J.: Globus pallidus internus deep brain stimulation for dystonic conditions: a prospective audit. Mov. Disord., **18**, 436–442 (2003)
14. Hung, S.W., et al.: Long-term outcome of bilateral pallidal deep brain stimulation for primary cervical dystonia. Neurology **68**, 457–459 (2007)
15. Loddenkemper, T., Pan, A., Neme, S., Baker, K.B., Rezai, A.R., Dinner, D.S., Montgomery, E.B. Jr., Lüders, H.O.: Deep brain stimulation in epilepsy. J. Clin. Neurophysiol. **18**, 514–532 (2001)
16. Stefurak, T., Mikulis, D., Mayberg, H., Lang, A.E., Hevenor, S., Pahapill, P., Saint-Cyr, J., Lozano, A.: Deep brain stimulation for Parkinson's disease dissociates mood and motor circuits: a functional MRI case study. Mov. Disord., **18**, 1508–1516 (2003)
17. Kringelbach, M.L., Jenkinson, N., Owen, S.L.F., Aziz, T.Z.: Translational principles of deep brain stimulation. Nat. Rev., Neurosci. **8**, 623–635 (2007)
18. Montgomery, E.B. Jr., Gale, J.T.: Mechanisms of action of deep brain stimulation (DBS). Neurosci. Biobehav. Rev. **32**, 388–407 (2008)
19. Jensen, A.L., Durand, D.M.: Suppression of axonal conduction by sinusoidal stimulation in rat hippocampus in vitro. J. Neural. Eng. **4**, 1–16 (2007)
20. Jensen, A.L., Durand, D.M.: High frequency stimulation can block axonal conduction. Exp. Neurol. **220**, 57–70 (2009)
21. Li, J., Andrews, R.J.: Trimodal nanoelectrode array for precise deep brain stimulation: prospects of a new technology based on carbon nanofiber arrays. Acta Neurochir., Suppl. **97**, 537–545 (2007)
22. FitzHugh, R.A.: Impulses and physiological states in theoretical models of nerve membrane. Biophys. J. **1**, 445–466 (1961)
23. Nagumo, J., Arimoto, S., Yoshizawa, S.: An active pulse transmission line simulating nerve axon. Proc. IRE **50**, 2061–2070 (1962)
24. Kevorkian, J.K., Cole, J.D.: Multiple Scale and Singular Perturbation Methods. Springer, New York (1996)
25. Scott, A.C.: The electrophysics of a nerve fiber. Rev. Mod. Phys. **47**, 487–533 (1975)
26. Keener, J.P.: Waves in excitable media. SIAM J. Appl. Math. **39**, 528–548 (1980)

27. Flores, G.: Stability analysis for the slow traveling pulse of the FitzHugh–Nagumo system. SIAM J. Math. Anal. **22**, 392–399 (1991)
28. Jones, C.K.R.T.: Stability of the travelling wave solution of the FitzHugh–Nagumo system. Trans. Am. Math. Soc. **286**, 431–469 (1984)
29. Keener, J.P., Sneyd, J.: Mathematical Physiology. Springer, New York (1998)
30. Dhooge, A., Govaerts, W., Kuznetsov, Yu.A.: MATCONT: a MATLAB package for numerical bifurcation analysis of ODEs. ACM Trans. Math. Softw. **29**, 141–164 (2003)
31. Miura, R.M.: Accurate computation of the stable solitary wave for the FitzHugh–Nagumo equations. J. Math. Biol. **13**, 247–269 (1982)